Multiparameter FWI: What Can Be Truly Unveiled from Pressure Data?

Guanghui Huang, Jaime Ramos-Martínez, Dan Whitmore and Carlos Calderón-Macías, TGS

Summary

There is growing interest in assessing the value of full waveform inversion (FWI) for applications beyond structural seismic imaging, particularly in marine environments where hydrophone data are predominant. Here, we first present a theoretical FWI framework for jointly estimating P-wave velocity (v_p), density (ρ) and S-wave velocity (v_s) from pressure measurements. We validate the approach with a controlled numerical experiment that simulates streamer acquisition in a deep-water setting. Our results indicate that, although updates to v_s and ρ predominantly capture local contrasts, elastic FWI can still recover meaningful variations in these parameters which are valuable for quantitative information. We apply our approach to field data acquired offshore Brazil. We validate our results from available well-log information.

Introduction

Elastic multiparameter FWI (eMP-FWI) has been recently used for applications beyond structural interpretation (e.g., Gomes et al., 2025; Shen et al., 2025). In this framework, Huang et al. (2026) showed that it is possible to estimate density contrasts negatively correlated with a corresponding velocity contrast characterized by a specific AVA anomaly. This in addition to the benefits in velocity model building and imaging that brings the join estimation of velocity and reflectivity in complex scenarios characterized by high impedance contrasts. In the work of Shen et al (2025), it is shown that angle dependent amplitude and phase information of the reflections in the hydrophone data can be used for resolving local variations of P- and S-wave velocity as well as for density

In this work, we describe the theory behind eMP-FWI parameterized in terms of v_p, v_s and density. We discuss the actual parameter information that can be estimated from pressure data using a controlled experiment. We then apply these findings in a field data application of narrow-azimuth data acquired with dual-sensor technology in offshore Brazil.

Theory

We depart from the elastodynamic equations in its stress-particle form

$$\rho \frac{\partial v_i}{\partial t} = \frac{\partial \sigma_{ij}}{\partial x_j} \quad (1)$$

$$\frac{\partial \sigma_{ij}}{\partial t} = c_{ijkl} \frac{\partial v_k}{\partial x_l} \quad (2)$$

where v_i is the particle velocity, σ_{ij} is the stress tensor, ρ is density, c_{ijkl} is the stiffness tensor and $i, j, k, l = 1,2,3$.

To derive the sensitive kernels for the stiffness tensor and density, we apply the adjoint-sate method. Note that the first-order formulation of elastodynamic equations (1)-(2) is not self-adjoint, in contrast to the forward modeling equation. This complicates the validation of the gradient accuracy and adds extra cost for backpropagation (Shen et al, 2025). In our implementation, the backpropagation wavefield is solved using the same forward equations (1)-(2), enabled by the compliance tensor $(c_{mnij})^{-1}$, i.e., the inverse of the stiffness tensor. This leads to the following sensitivity kernels for the stiffness tensor and density:

$$\nabla_\rho J = \sum_i \int_0^T \frac{\partial v_i}{\partial t} w_i dt \quad (3)$$

$$\nabla_{c_{ijkl}} J = -\int_0^T \frac{\partial v_k}{\partial x_l} (c_{mnij})^{-1} \tau_{mn} dt \quad (4)$$

where w_i and τ_{ij} are the corresponding backpropagated wavefields solving equations (1)-(2) backward in time. Invoking the chain rule, we derive the sensitivity kernels for P- and S-wave velocities (v_p, v_s) and density (ρ),

$$\nabla_{v_p} J = \sum_{i,j,k,l} \int_0^T \frac{\partial v_k}{\partial x_l} (c_{i'j'ij})^{-1} (\partial_{v_p} c_{m'n'i'j'}) (c_{mnm'n'})^{-1} \tau_{mn} dt \quad (5)$$

$$\nabla_{v_s} J = \sum_{i,j,k,l} \int_0^T \frac{\partial v_k}{\partial x_l} (c_{i'j'ij})^{-1} (\partial_{v_s} c_{m'n'i'j'}) (c_{mnm'n'})^{-1} \tau_{mn} dt \quad (6)$$

$$\nabla_\rho J = \sum_i \int_0^T \frac{\partial v_i}{\partial t} w_i dt + \sum_{i,j,k,l} \int_0^T \frac{\partial v_k}{\partial x_l} (c_{i'j'ij})^{-1} (\partial_\rho c_{m'n'i'j'}) (c_{mnm'n'})^{-1} \tau_{mn} dt \quad (7)$$

where $\partial_{v_p} c_{m'n'i'j'}$, $\partial_{v_s} c_{m'n'i'j'}$ and $\partial_\rho c_{m'n'i'j'}$ are the derivatives of the stiffness tensor with respect to v_p, v_s and ρ, respectively.

Synthetic example

We validate our approach with a controlled experiment using a modified version of the 3D overthrust model, adding a water layer at the top of the model and setting sources and receivers in the water to simulate a streamer acquisition. Figure 1a shows the true v_p model, which includes a box inclusion, and Figure 1b shows the initial v_p model, a smoothed version of the true model without the inclusion. The true and initial v_s models were computed from empirical relations without inclusions. The true ρ is built based on Gardner's law without the inclusion and the initial density is smoothed version of the true density. The maximum frequency for inversion is 15 Hz, and the maximum offset is 8 km. In Figures 1c, 1e and 1g, we show the actual difference between true and initial models, while Figures 1d, 1f and 1h show corresponding inverted v_p, v_s and ρ model updates, respectively, obtained from the simultaneous inversion. The inverted v_p model, in Figure 1d, recovers most of actual updates including the box inclusion depicted in Figure 1c. The inverted velocity updates for v_p exhibits low-wavenumber content compared with those obtained for v_s (Figure 1f).

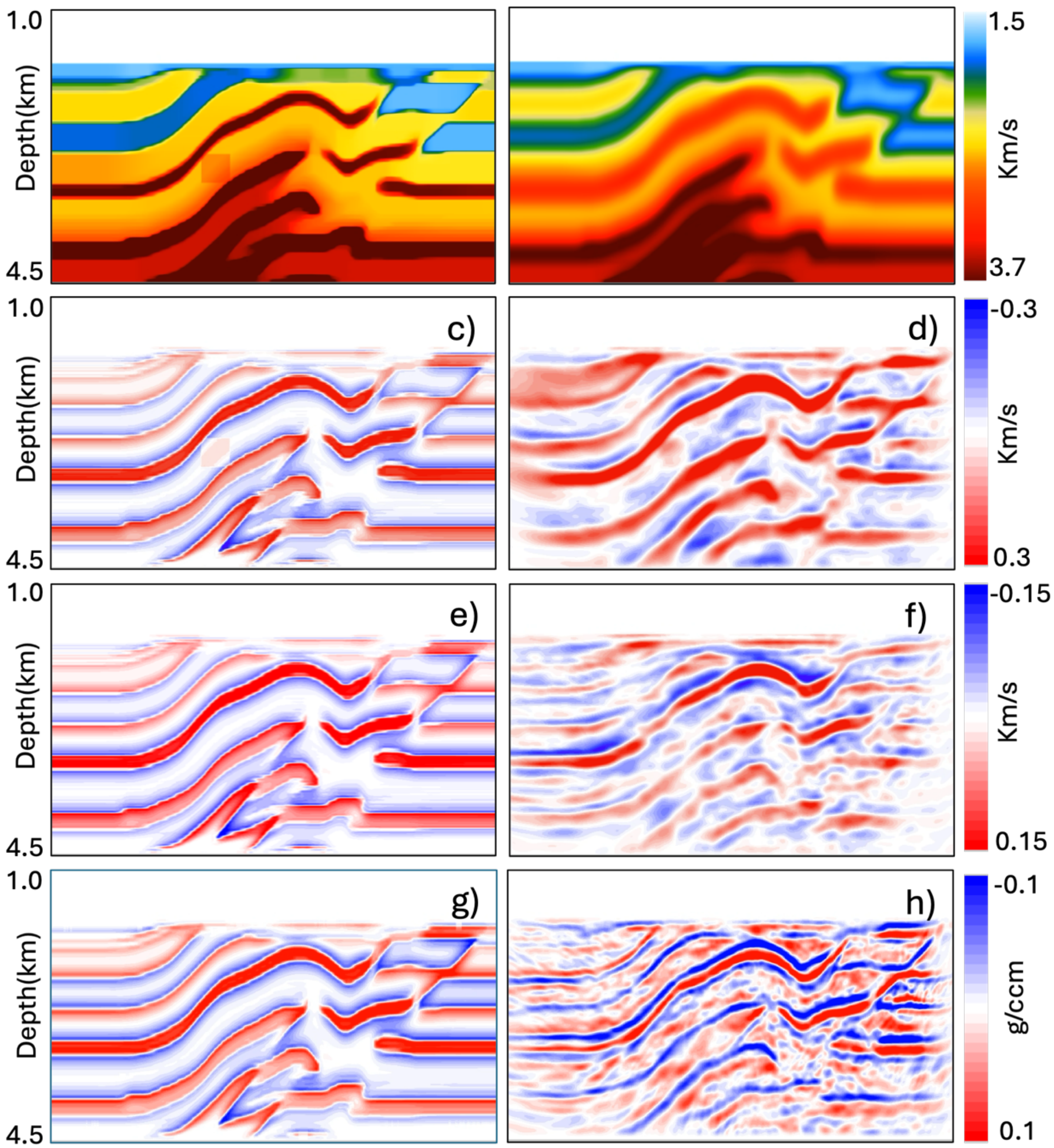

Figure 1. Synthetic example using a modified version of the overthrust model. a) True and b) initial v_p model. True updates for c) v_p, e) v_s and g) density. Updates for inverted d) v_p, f) v_s and h) density.

Density (ρ) updates contain mostly high-wavenumber features. A similar observation was made by Shen et al. (2025), who explained it by comparing the ρ sensitivity kernel with the inverse scattering imaging condition used in RTM (Whitmore and Crawley, 2012).

Field data example

We illustrate the performance of our inversion with streamer data acquired with dual-sensor technology in offshore deep-water Brazil. Since v_p is the most robust parameter to estimate from pressure data, our first objective is to have an accurate estimate of v_p.

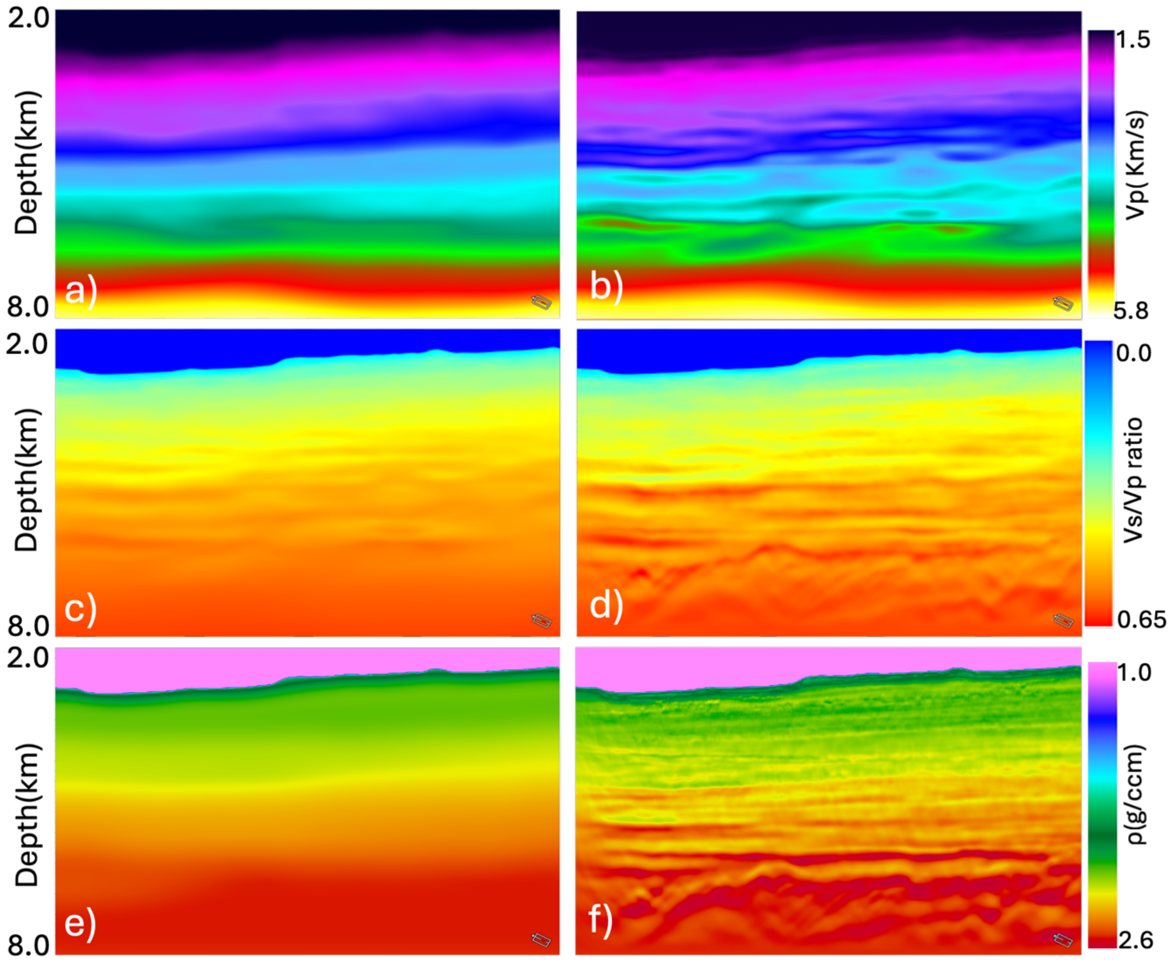

Figure 2. Field data eMP-FWI example in deep-water offshore Brazil. Initial a) v_p, c) v_s/v_p and e) density models. Inverted b) v_p, d) v_s/v_p and e) density models.

The initial v_p model (Figure 2a) was constructed using reflection tomography, which also provided a reliable estimate of the anisotropic parameters. The velocity model was then refined through eMP-FWI using a velocity and reflectivity parameterization as described in Huang (2026), which enabled the scale separation between v_p and reflectivity impact (and avoid density contamination). Because this is a deep-water setting, reflectivity modeling is used for producing the corresponding seismic events to match the recorded data during inversion. The inverted v_p model (Figure 2b) matches well the sonic logs available in the area. Once v_p is accurate enough, we focus in updating v_s and ρ. The initial v_s and density models were computed from empirical relations from the updated v_p. The initial v_s/v_p ratio model is displayed in Figure 2c. The initial density model (Figure 2e) was heavily smoothed aiming to detect density contrast variations from the data and independent of high wavenumber velocity updates. From the results, we observe that v_s and density updates depend mostly on the amplitude and phase signatures of the P-wave reflectivity, as previously discussed by Shen et al. (2025). These signatures vary with incident angle and are produced by localized contrasts in v_s and density. Figure 2d shows the final v_s/v_p from inverting v_s, while Figure 2f shows the inverted ρ model, which exhibits high wavenumber features consistent with those observed in our controlled experiment.

To validate our results, Figure 3 presents a comparison between raw logs and the inverted profiles for v_p, v_s/v_p and density at a well location. The eMP-FWI workflow improves the agreement of the v_p and v_s/v_p profiles with the corresponding well-logs when compared with the initial models. For density, the inversion captures negative density contrasts observed in the well log, particularly in the case of a class IIp AVA anomaly.

Conclusions

We introduce a new elastic multiparameter FWI implementation for estimating v_p, v_s and ρ with pressure-only data. The proposed parameterization and workflow can recover local variations in v_s and ρ from seismic signatures present in P-wave reflectivity, in addition to the construct of the v_p field traditionally inverted with single-parameter inversions. These localized variations provide valuable quantitative information for reservoir characterization. We demonstrate the effectiveness of the approach using streamer data acquired in deep-water offshore Brazil. The results are validated by the good agreement between the inverted profiles and the corresponding well logs.

Acknowledgements

We thank TGS for permission to publish this material. We thank Multiclient TGS for authorization to use the field dataset. We thank our colleagues in R&D Geophysics for valuable discussions.

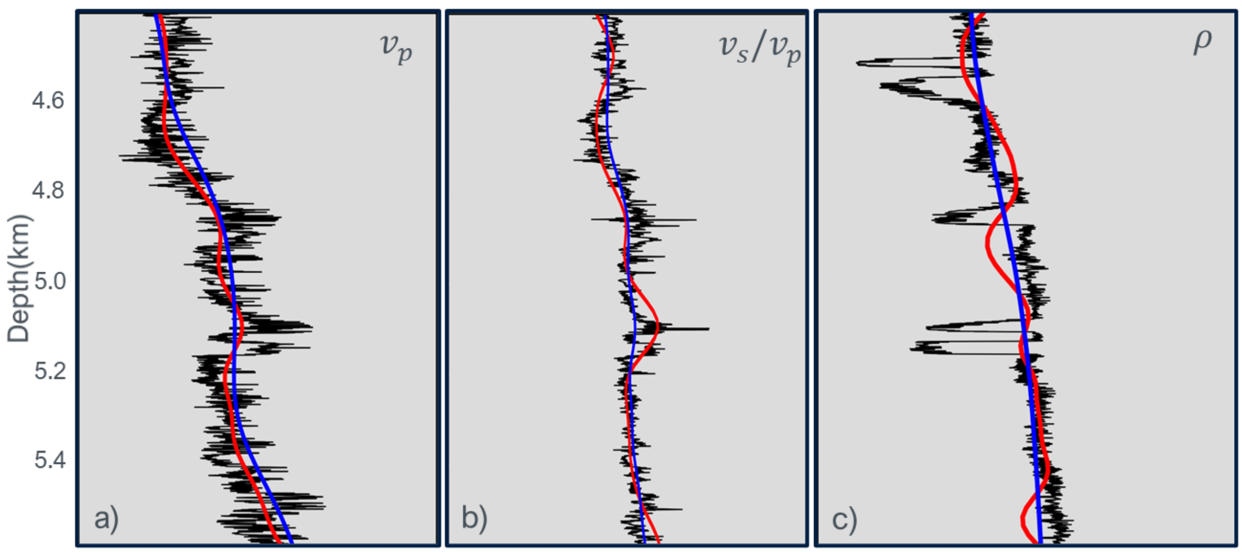

Figure 3. Field data eMP-FWI example. Comparison of the initial (blue line) and inverted (red line) profiles with the well-logs (black line) for a) v_p, b) v_s/v_p and c) density.